Accreting matter around clusters of galaxies: one-dimensional considerations

Dongsu Ryu[1]★ and Hyesung Kang[2]★

[1]*Department of Astronomy & Space Science, Chungnam National University, Daejeon 305-764, Korea*
[2]*Department of Earth Sciences, Pusan National University, Pusan 609-735, Korea*

ABSTRACT
During the formation of large-scale structure in the Universe, matter accretes on to high-density peaks. Accreting collisionless dark matter (DM) forms caustics around them, while accreting collisional baryonic matter (BM) forms accretion shocks. The properties of the accreting matter depend upon the power spectrum of the initial perturbations on a given scale as well as the background expansion in a given cosmological model. In this paper, we have calculated the accretion of DM particles in one-dimensional spherical geometry under various cosmological models including the Einstein–de Sitter universe, the open universe with $\Omega_0 < 1$, and the flat universe with $\Omega_\Lambda = 1 - \Omega_0$. A density parameter in the range $0.1 \leq \Omega_0 \leq 1$ has been considered. The initial perturbation characterized by a point mass at the origin has been considered. Since the accretion shock of BM is expected to form close to the first caustic of DM, the properties of the accreting BM are common with those of the DM. Hence, the accretion calculations with DM particles have been used to find the position and velocity of the accretion shock and the cluster mass inside it. The average temperature of BM has been estimated by adopting simplifying assumptions. The velocity of the accreting BM around clusters of a given temperature is lower in a universe with lower Ω_0, but only by up to ~ 24 per cent in the models with $0.1 \leq \Omega_0 \leq 1$. Thus, it would be difficult to use that quantity to discriminate among the cosmological models. However, the accretion velocity around clusters of a given mass or a given radius depends more sensitively on the cosmological models. It is lower in a universe with lower Ω_0 by up to ~ 41 and ~ 65 per cent, respectively. So, it can provide a better signature of the background expansion for different cosmological models. Although the existence of the caustics and the accretion shocks may not be confirmed by direct X-ray observations, the infalling warm gas of 10^4–10^5 K upstream of the shocks may be observed as the absorption systems of quasar emission lines. According to this study, the suggestion made by Kang, Ryu & Jones that the large-scale accretion shocks around clusters of galaxies can serve as possible acceleration sites of ultrahigh-energy cosmic rays above 10^{18} eV remains plausible in all viable cosmological models.

Key words: cosmic rays – galaxies: clusters: general – dark matter.

1 INTRODUCTION

Recent satellite X-ray observations have made clusters of galaxies increasingly important to cosmology as a probe into the large-scale structure of the Universe. Being massive and

rare, their abundance in the local and distant Universe carries vital information on the initial density fluctuations and the matter content of the Universe (Lubin et al. 1996; Eke, Cole & Frenk 1996). Also being relatively young dynamically, the details of their structures can provide us with some signatures left over from the formation epoch as well as information on the background cosmology (Crone, Evrard & Richstone 1994; Navarro, Frenk & White 1995; Tsai &

★E-mail: ryu@sirius.chungnam.ac.kr (DR);
kang@astrophys.es.pusan.ac.kr (HK)

Buote 1996). A general consensus seems to be that the standard cold dark matter (CDM) model (i.e., $\Omega = 1$ and $h = 0.5$) normalized to the *COBE* DMR measurement of the anisotropies in the cosmic background radiation (i.e., $\sigma_8 > 1$) has serious difficulties in explaining the observed properties of X-ray clusters, such as the cluster abundance (Kang et al. 1994), the baryon fraction in clusters (Lubin et al. 1996), and the contribution of cluster emission to the X-ray background (Kang et al. 1994; Kitayama & Suto 1996). On the other hand, an open or a flat CDM model with a cosmological constant with a smaller value of σ_8 seems more consistent with many observations, and so has become popular recently (Cen & Ostriker 1994; Ostriker & Steinhardt 1995).

Although the application of the Press–Schechter formalism (Press & Schechter 1974) to the hierarchical clustering model of cluster formation has been successful in getting good agreement with the results of *N*-body simulations (Lacey & Cole 1994), this semi-analytic approach cannot include the effects of non-equilibrium hydrodynamics that could be important during some phases in cluster evolution (Kang et al. 1994). Some studies suggest that the amplitude of the density power spectrum, σ_8, can be constrained by the local cluster abundance (Eke, Cole & Frenk 1996; Viana & Liddle 1996) and the range of the allowed value of Ω_0 can be narrowed down by examining the evolution of cluster abundance at low redshifts (i.e., $z < 1$) (Bahcall & Cen 1992; White, Efstathiou & Frenk 1993). Despite this, the observational and theoretical/numerical errors involved in such procedures seem to be too big to make any consistent predictions on those key cosmological parameters (Castander et al. 1995; Luppino & Gioia 1995; Tsai & Buote 1996). It is also unlikely that all crucial physics can be included in any variants of the treatments.

The properties of X-ray clusters, other than the abundance and the baryon fraction mentioned above, which have been investigated for various cosmological models, include the cluster–cluster correlation function (Bahcall & Cen 1992), the density and velocity profiles (Crone, Evrard & Richstone 1994), and the degree of substructures in the intracluster medium (ICM) (Tsai & Buote 1996). The latter two, associated with the internal structure of clusters, are closely related with recent mergers and accretion on to the cluster mass-scale ($\sim 8 \, h^{-1}$ Mpc), so dependences on Ω, n (the power-law index of the initial power spectrum), and σ_8 could be degenerate. In addition to that, statistical treatments of observed data of those quantities have a harder time discriminating clearly among different cosmological models compared with the statistics of the cluster abundance. Even though there are tantalizing possibilities that the various properties of X-ray clusters can indeed be used to unveil the fundamental nature of the Universe, further improvements by a factor of at least a few in both theoretical and observational fronts seem to be required in order to make some solid predictions.

In this paper, we have examined one more physical property associated with X-ray clusters, the accretion flow infalling toward the clusters. Matter accretes on to the high-density peaks continuously throughout the history of the Universe. Its rate on the scale of the cluster mass will be determined by the initial density fluctuations and the background cosmology. Fluctuations continue to grow in the

$\Omega = 1$ universe, while they stop growing at a redshift $z \sim \Omega_0^{-1} - 1$ in a universe with low Ω_0 (Peebles 1993). On the other hand, the accretion on larger scales gets stronger for a smaller n for a scale-free power spectrum. Crone, Evrard & Richstone (1994) examined the radial velocity profile of the accretion flow through *N*-body simulations of different cosmological models with scale-free power spectra. They found that the density profile is flatter and the accretion regime is stronger for higher Ω_0 and smaller n.

If the initial density perturbation is scale-free, the accretion of both baryonic matter and dark matter in the $\Omega_0 = 1$ universe can be described semi-analytically with a self-similar solution (Fillmore & Goldreich 1984; Bertschinger 1985). However, in a universe with $\Omega_0 \neq 1$, the self-similar solution is not possible, since, in addition to the time-scale marking the transition of the initial perturbation to the non-linear regime, another time-scale such as the cosmic time $t_{1/2}$ when $|1 - \Omega| = 1/2$ enters the problem.

Here, we use a one-dimensional spherical *N*-body code, which can follow the evolution of collisionless dark matter particles, to find the properties of accretion flows on to objects of cluster mass-scales in different cosmological models: the Einstein–de Sitter universe with $\Omega_0 = 1$, the low-density, open universe with $\Omega_0 < 1$, and the low-density, flat universe with $\Omega_0 < 1$ and $\Omega_\Lambda = 1 - \Omega_0$ (from non-zero cosmological constant, Λ). While most previous studies on accretion focused on the density profile inside the collapsed objects developed from infall, our primary interests lie in the properties of spherical accretion flows outside the objects. In the accretion of both dark matter (DM) and baryonic matter (BM), the collisionless DM forms caustics around the overdensity, while the collisional BM forms accretion shocks stopping the infalling material. In this situation, as pointed out by Bertschinger (1985), the position of the accretion shock of the gas with $\gamma = 5/3$ is very close to the position of the first caustic of the DM particles. In addition, since in the region outside the shock the accretion solution for BM is almost identical to that for DM, the infall velocity of BM upstream of the accretion shock can be described by that of the DM. Hence, hydrodynamic calculations to follow BM are not necessary if we are interested only in the position of the accretion shocks and the properties of the accretion flows.

Of course, one-dimensional treatments cannot include important physics such as virialization in the central region. Three-dimensional simulations (Kang et al. 1994; Navarro, Frenk & White 1995; Evrard, Metzler & Navarro 1996) showed that the gas is shock-heated to the virial temperature and then settles into hydrostatic equilibrium (HSE) and that the shock separates the hydrostatic central region from the infalling flow. However, according to Navarro, Frenk & White (1995), where *N*-body smoothed particle hydrodynamics (SPH) simulations were used to examine the properties of X-ray clusters in the $\Omega = 1$ CDM universe, the one-dimensional, self-similar solution of Bertschinger (1985) matches well the density and temperature profiles of their simulated clusters except for the inner central region. Thus, the properties of accretion flow can be efficiently studied by one-dimensional calculations.

The plan of the paper is as follows. In Section 2 we present the results focusing on the velocity of the accretion flows. In Section 4 we discuss the implications of the results

on cosmology and on cosmic-ray acceleration by the accretion shocks. Details such as the evolution equations and the numerical scheme are given in the appendices.

2 SIMULATIONS

We follow the evolution of collisionless DM particles accreting on to an initial density enhancement in an otherwise homogeneous universe through calculations with a spherical *N*-body code. The equations describing the particle motion and gravity in comoving coordinates and the expansion of the background universe can be found, for example, in Peebles (1993) and are summarized in Appendix A. The details of our numerical code are described in Appendix B.

The calculations start at the time corresponding to the initial expansion parameter $a_i = 10^{-5} a_0$ with 10^4 particles. Initially the particles are at rest and distributed uniformly, except for an excess mass at the origin to initiate the collapse. So the initial perturbation can be characterized by the *point-mass* perturbation

$$\frac{\delta M(r)}{M(r)} = \left(\frac{M(r)}{M_0}\right)^{-1}, \tag{1}$$

where $M(r)$ is the mass inside a radius r and M_0 is a reference mass. Note that the point-mass perturbation can be approximated by the constant power spectrum (i.e., $P(k) \approx$ constant with $n=0$) (Hoffman & Shaham 1985). Although a scale-free power spectrum with $n = -1$ would represent better the CDM power spectrum on the cluster scale (see for example, Bardeen et al. 1986 for the CDM power spectrum), the constant power spectrum would be a better approximation on scales a bit larger than that. Also according to Navarro, Frenk & White (1995), the self-similar solution of Bertschinger (1985) with the above initial perturbation represents well the structures of simulated clusters in an $\Omega = 1$ universe with the CDM power spectrum except for the inner central region. The amount of the excess mass, M_0, has been chosen so that at the present epoch about 1/3 of the particles are placed inside the first caustic. It requires an excess mass corresponding to 1–2 particles.

Note that the present value of the Hubble parameter, or $h \equiv H_0/100$ km s^{-1} Mpc^{-1}, enters the problem only through the normalization parameters such as $t_0 \propto 1/h$, $L_0 \propto 1/h$, and $\bar{\rho} \propto h^2$ (see the appendices). So, we can include the dependence on h implicitly by expressing the results in terms of $t_0 h$, $L_0 h$, and $\bar{\rho} h^{-2}$ (or equivalently $M_0 h$).

If we had followed the evolution of BM with $\gamma = 5/3$ as well, its accretion shock would have occurred very close to the first caustic of DM and its accretion velocity outside the shock would have been very similar to that of DM outside the first caustic. Since the accretion shock approximately separates the inner virialized region from the outer infalling flow, here we will consider a cluster to be the region inside the first caustic. So, below, we define the radius of the first caustic, R_{cl}, as the cluster radius, the mass inside R_{cl}, M_{cl}, as the total cluster mass, and the particle velocity just outside R_{cl}, v_{acc}, as the cluster accretion velocity.

Our numerical set-up has been designed in a way parallel to that of Bertschinger (1985), so our numerical solution for

the $\Omega = 1$ case should be identical to his self-similar solution. Thus, the accuracy of our code has been tested against his solution. Fig. 1 shows the present phase-space distribution of particles in the Einstein–de Sitter universe, which can be directly compared with fig. 6 of Bertschinger (1985). The variables used in the plot are related to those in the appendices as follows

$$\lambda = \frac{r}{r_{ta}}, \tag{2}$$

$$\frac{d\lambda}{d\xi} = (u + \dot{a}_0 r)\frac{t_0}{r_{ta}} - \frac{8}{9}\lambda, \tag{3}$$

where r_{ta} is the present turnaround radius. Our smoothing length in the gravitational force corresponds to $\lambda_{sm} = 0.0936$ (see Appendix B). The plot shows that the numerical solution for $\lambda \gtrsim \lambda_{sm}$ agrees well with the exact analytic solution. The position of the first caustic agrees well with that of the analytic solution and the accretion velocity outside it agrees almost exactly. On the other hand, for $\lambda \lesssim \lambda_{sm}$ the agreement in the two solutions is not so good. The numerical solution has given a lower velocity than the analytic one and the positions of caustics have not been calculated correctly, as expected. However, the quantities we are interested in, R_{cl}, M_{cl}, and v_{acc}, are less affected by the smoothing. Comparison of Fig. 1 with fig. 6 of Bertschinger (1985) shows that these quantities have been calculated accurately within an error typically less than 5 per cent or so.

Fig. 2 shows the evolution of the mass, radius, and accretion velocity of a cluster with the present mass of $M_{cl}(z=0) = 10^{15} \ h^{-1} \ M_\odot$ as a function of redshift in the Einstein–de Sitter universe, in the open universe with $\Omega_0 = 0.2$, and in the flat universe with $\Omega_0 = 0.2$. The dotted lines represent the power-law evolution of the analytic solution in the Einstein–de Sitter universe (Bertschinger 1985);
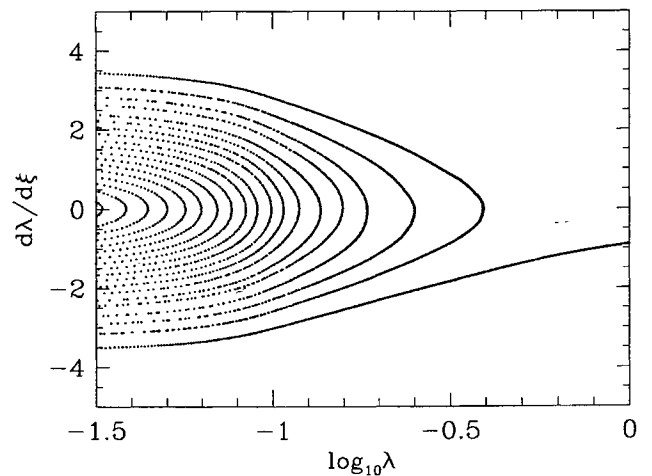

Figure 1. Present phase-space distribution of DM particles from the numerical calculation in the Einstein–de Sitter universe. It has been drawn for direct comparison with fig. 6 of Bertschinger (1985). The relations of the variables used in the plot to those in the appendices are $\lambda = r/r_{ta}$ and $d\lambda/d\xi = (u + \dot{a}_0 r)(t_0/r_{ta}) - (8/9)\lambda$. Here, r_{ta} is the present turnaround radius.
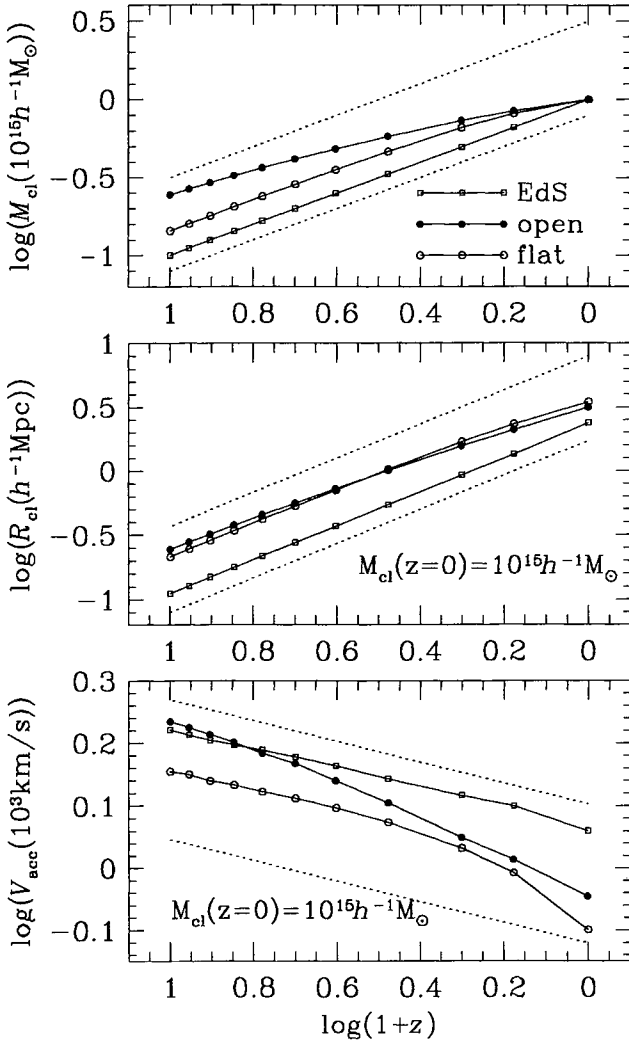
Figure 2. Evolution of the radius, mass, and accretion velocity of a cluster with the present mass $M_{cl}(z=0) = 10^{15} h^{-1} M_\odot$ as a function of redshift in the Einstein–de Sitter universe (open squares), in the open universe with $\Omega_0 = 0.2$ (filled circles), and in the flat universe with $\Omega_0 = 0.2$ (open circles). The dotted lines represent the power-law evolution in the exact self-similar solution in the Einstein–de Sitter universe (Bertschinger 1985).

$M_{cl} \propto (1+z)^{-1}$, $R_{cl} \propto (1+z)^{-4/3}$, and $v_{acc} \propto (1+z)^{1/6}$. The numerical solution in the Einstein–de Sitter universe follows the self-similar evolution very closely. Again, good agreement of the numerical solution with the analytic solution indicates that our code has been able to calculate the quantities used in this paper reliably. But those in other model universes do not show the power-law evolution in $(1+z)$, indicating the absence of the self-similarity.

3 RESULTS

Among the quantities we can extract from the X-ray observations of clusters, the ICM temperature T_x (usually averaged over a core region) is the one that can be estimated most reliably in hydrodynamic numerical simulations and that is less prone to numerical effects such as the problem of

under-resolved structure. That is because T_x is a conserved quantity per unit mass (i.e. the specific thermal energy). Although clusters have formed only recently ($z < 1$) and the dynamical time of cluster evolution is about the Hubble time, the structure of more-or-less relaxed clusters both in observations and simulations is well represented by the virialized region in HSE with nearly constant temperature (Forman & Jones 1982; Evrard et al. 1996). Exceptions are the clusters that have recently undergone mergers. Under the assumption of an *isothermal sphere in HSE*, the average temperature is proportional to $M(<r)/r$, or to the galactic kinetic energy per unit mass, σ_v^2. So we use the ratio of the total cluster mass to radius, M_{cl}/R_{cl}, as a quantity to represent the observed, average temperature (emission weighted). As shown by three-dimensional simulations (Navarro, Frenk & White 1995; Evrard et al. 1996), simulated clusters of different masses have similar structures when they are scaled with a radius of a fixed density contrast ($\delta = \bar{\rho}/\rho_{crit} \gtrsim 200$). So the temperature follows the scaling law, $T \propto M(<r_c)/r_c \propto r_c^2$, where r_c is the characteristic radius at a fixed density contrast. Of course, the constant of proportionality for this scaling relation varies for different cosmologies.

Here, we use the quantities, M_{cl}, R_{cl}, or M_{cl}/R_{cl}, to denote clusters. Note that R_{cl} corresponds to the characteristic radius of $\delta \sim 80$. Under the set-up considered in this paper, only one of them is independent in a given cosmological model universe, because of the similarity in cluster structure. According to Bertschinger (1985), the self-similar solution at the present epoch in the Einstein–de Sitter universe gives

$$R_{cl} = 2.22\, h^{-1}\, \text{Mpc} \left(\frac{M_{cl}}{10^{15}\, h^{-1}\, M_\odot} \right)^{1/3}, \quad (4)$$

$$R_s = 2.12\, h^{-1}\, \text{Mpc} \left(\frac{M_{cl}}{10^{15}\, h^{-1}\, M_\odot} \right)^{1/3}, \quad (5)$$

$$T_{cl}(0.3R_s) = 6.06\, \text{keV} \left(\frac{M_{cl}}{10^{15}\, h^{-1}\, M_\odot} \right)^{2/3}, \quad (6)$$

$$v_{acc} = 1.31 \times 10^3\, \text{km s}^{-1} \left(\frac{M_{cl}}{10^{15}\, h^{-1}\, M_\odot} \right)^{1/3}. \quad (7)$$

Here R_s is the shock radius, and T_{cl} is the temperature at $r = 0.3R_s$, which we may take as an average ICM temperature of the self-similar flow. Navarro, Frenk & White (1995) showed that the temperature profiles of simulated clusters normalized with the temperature at r_{200} of $\delta = 200$ can be represented within a factor of two by that of the self-similar solution of Bertschinger (1985) in $r/r_{200} \gtrsim 0.3$. In the core region within $r/r_{200} < 0.3$, the temperature is approximately isothermal. Thus, T_{cl} should be a reasonable approximation to the average temperature of the cluster core region.

In Fig. 3 we have plotted the present M_{cl}/R_{cl} for clusters with the present mass $M_{cl}(z=0) = 10^{15}\, h^{-1}\, M_\odot$ (upper panel) and for clusters with the present radius $R_{cl}(z=0) = 2.5\, h^{-1}$ Mpc (lower panel) in the open models and flat models with $\Omega_0 \leq 1$ against the values of Ω_0. Those with $\Omega_0 = 1$ correspond to the values in the Einstein–de
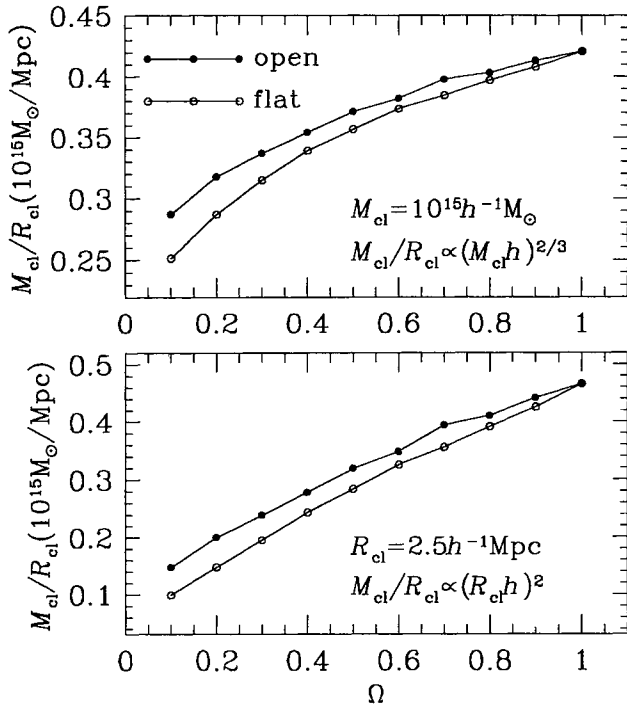
Figure 3. Present M_{cl}/R_{cl} for clusters with the present mass $M_{cl}(z=0)=10^{15}\ h^{-1}\ M_\odot$ (upper panel) and for cluster with the present radius $R_{cl}(z=0)=2.5\ h^{-1}$ Mpc (lower panel) in the open universes (filled circles) and the flat universes (open circles) with different Ω_0. That with $\Omega_0=1$ represents the values in the Einstein–de Sitter universe.
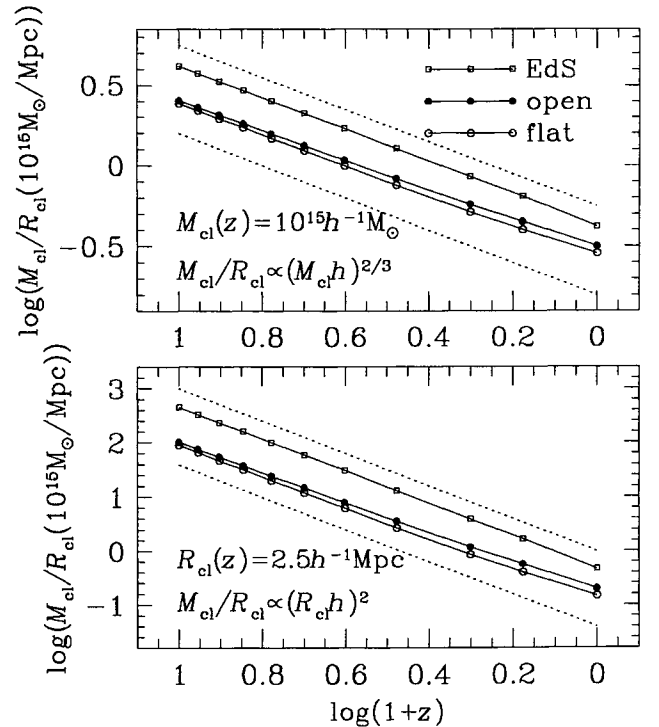
Figure 4. M_{cl}/R_{cl} as a function of redshift in the Einstein–de Sitter universe (open squares), in the open universe with $\Omega_0=0.2$ (filled circles), and in the flat universe with $\Omega_0=0.2$ (open circles). The upper panel is for clusters with a mass at given z, $M_{cl}(z)=10^{15}\ h^{-1}$ $M_\odot$. The lower panel is for clusters with a radius at given z, $R_{cl}(z)=2.5\ h^{-1}$ Mpc. The dotted lines represent the power-law evolution in the exact self-similar solution in the Einstein–de Sitter universe (Bertschinger 1985).

Sitter universe. Here we have chosen $R_{cl}=2.5\ h^{-1}$ Mpc as a fiducial value of the first caustic, since the typical radius of cluster core regions is often defined as $r_{core}=0.5\ h^{-1}$ Mpc and the Abell radius is $R_A=1.5\ h^{-1}$ Mpc. According to the self-similar solution of Bertschinger (1985) given above, in the Einstein–de Sitter universe,

$$\frac{M_{cl}}{R_{cl}}=4.51\times10^{14}\ \frac{M_\odot}{\mathrm{Mpc}}\left(\frac{M_{cl}}{10^{15}\ h^{-1}\ M_\odot}\right)^{2/3} \tag{8}$$

for clusters with the given mass, while

$$\frac{M_{cl}}{R_{cl}}=5.73\times10^{14}\ \frac{M_\odot}{\mathrm{Mpc}}\left(\frac{R_{cl}}{2.5\ h^{-1}\ \mathrm{Mpc}}\right)^2 \tag{9}$$

for clusters with the given radius. Comparison between these values and our numerical results for $\Omega_0=1$ case shows about ~10 per cent error. Since M_{cl}/R_{cl} scales as $M_{cl}/R_{cl}\propto(M_{cl}h)^{2/3}$ for clusters with different masses and $M_{cl}/R_{cl}\propto(R_{cl}h)^2$ for clusters with different radii, the results can be scaled accordingly.

The figure shows that the clusters, if they have the same mass or the same radius, are less tightly bound, and so have lower M_{cl}/R_{cl} in the universe with lower Ω_0. Also, the clusters are less tightly bound in the flat universe with non-zero Λ than in the open universe, if Ω_0 is the same. This is as a result of the fact that the background expands faster in the flat universe with non-zero Λ than in the open universe. In the open universe with $\Omega_0=0.1$, M_{cl}/R_{cl} is ~32 per cent and

~68 per cent lower than that in the Einstein–de Sitter universe for clusters with given mass and radius, respectively. In the flat universe with $\Omega_0=0.1$, M_{cl}/R_{cl} is ~40 per cent and ~79 per cent lower. This means that clusters are less massive and less bound so the ICM temperature is lower in low-density universes than in high-density universes, if they are selected by a constant radius criterion.

Fig. 4 shows the value of M_{cl}/R_{cl} as a function of redshift in the Einstein–de Sitter universe, in the open universe with $\Omega_0=0.2$, and in the flat universe with $\Omega_0=0.2$. The upper panel is for clusters the mass of which is $M_{cl}(z)=10^{15}\ h^{-1}$ $M_\odot$ at a given z. Similarly, the lower panel is for clusters the radius of which is $R_{cl}(z)=2.5\ h^{-1}$ Mpc at a given z. Thus, each point in the plots represent different clusters that should become heavier than $10^{15}\ h^{-1}\ M_\odot$ or bigger in radius than $2.5\ h^{-1}$ Mpc at the present epoch. In other words, the redshift dependences in these plots do not represent the evolution of a particular cluster in a 'Lagrangian' sense. They tell us that clusters selected by either a constant mass or a constant radius criterion would be more tightly bound and so hotter in the past (at higher redshifts) than at the present epoch in all cosmologies. The dotted lines represent the power-law redshift dependences [$M_{cl}/R_{cl}\propto(1+z)$ for clusters with a constant mass, and $M_{cl}/R_{cl}\propto(1+z)^3$ for clusters with a constant radius] of the self-similar solution in the Einstein–de Sitter universe. The numerical solution in the

Einstein–de Sitter universe follows the self-similar solutions very well. Once again we can see that clusters are less tightly bound in lower density universes. The increases of M_{cl}/R_{cl} with increasing redshift in both lower density universes are slightly less than that in the Einstein–de Sitter universe.

In Fig. 5 we plotted the accretion velocity, v_{acc}, for clusters with the present mass $M_{cl}(z=0)=10^{15}\,h^{-1}\,M_\odot$ (the first panel), for clusters with the present radius $R_{cl}(z=0)=2.5$ h^{-1} Mpc (the second panel), and for clusters with the present $M_{cl}/R_{cl}(z=0)=4\times10^{14}\,M_\odot\,\mathrm{Mpc}^{-1}$ (the third panel) in the open and flat universes with different $\Omega_0 s$. Note that $M_{cl}/R_{cl}=4\times10^{14}\,M_\odot\,\mathrm{Mpc}^{-1}$ corresponds to $T_{cl}=5.71$ keV in the Einstein–de Sitter universe (see equation 6) (corresponding T_{cl} should be slightly lower in the low-density universes). Clusters with different masses, radii, and $M_{cl}/R_{cl}s$ have the accretion velocity which scales as $v_{acc}\propto(M_{cl}h)^{1/3}$, $v_{acc}\propto R_{cl}h$, and $v_{acc}\propto(M_{cl}/R_{cl})^{1/2}$. Lower accretion velocity in

the universes with lower Ω_0 is consistent with the fact that the clusters are less tightly bound. The accretion velocity is slightly lower in the flat universe than in the open universe, if Ω_0 is the same. The plot shows that the accretion velocity of clusters with a given mass or a given radius is lower by up to ~ 41 and ~ 65 per cent respectively in the flat universe with $\Omega_0=0.1$ than in the Einstein–de Sitter universe.

For clusters with the same M_{cl}/R_{cl}, however, the difference between different cosmological models is rather small. In the open universe with $\Omega_0=0.1$ the accretion velocity is ~ 15 per cent lower than that in the Einstein–de Sitter universe, while in the flat universe with $\Omega_0=0.1$ it is lower by ~ 24 per cent. This means we can expect that the clusters with the same observed temperature can have accretion velocities lower by only up to ~ 25 per cent in low-density universes depending on Ω_0.

Fig. 6 shows the accretion velocity for clusters with a mass of $M_{cl}(z)=10^{15}\,h^{-1}\,M_\odot$ at given z (first panel), for clusters with a radius of $R_{cl}(z)=2.5$ h^{-1} Mpc at given z (second panel), and for clusters with $M_{cl}/R_{cl}(z)=4\times10^{14}\,M_\odot$ Mpc at a given z (third panel) in the Einstein–de Sitter universe, in the open universe with $\Omega_0=0.2$, and in the flat universe with $\Omega_0=0.2$. As in Fig. 4, they do not represent the evolutionary path of a cluster, but they show the dependence of v_{acc} on the redshift in a sample of clusters selected by a constant mass, or a constant radius, or a constant temperature criterion. The dotted lines represent the power-law dependence on the redshift of the self-similar solution in the Einstein–de Sitter universe, $v_{acc}\propto(1+z)^{1/2}$ for clusters with a constant mass, $v_{acc}\propto(1+z)^{3/2}$ for clusters with a constant radius, $v_{acc}\propto$ constant for clusters with a constant M_{cl}/R_{cl}.

The first two panels show that the accretion velocity of clusters with a constant mass or a constant radius was significantly larger in the past than now. On the other hand, the third panel shows that the accretion velocity of clusters with a constant M_{cl}/R_{cl} remains constant with redshift in the Einstein–de Sitter universe because of the scale-free nature. However, it was larger at high redshifts in the model universes with $\Omega_0<1$. For instance, in the open universe with $\Omega_0=0.2$ the accretion velocity was larger by ~ 8 per cent at high redshifts, while in the flat universe with $\Omega_0=0.2$ it was larger by ~ 18 per cent. At high redshifts ($z>5$) the difference in v_{acc} among different cosmological models considered here reduces to only a few per cent.

4 SUMMARY AND DISCUSSION

In this paper, we have studied the properties of spherically accreting flows onto an initially overdense perturbation in different cosmological model universes including the Einstein–de Sitter universe with $\Omega_0=1$, the low-density open universe with $\Omega_0<1$, and the low-density, flat universe with $\Omega_0<1$ and $\Omega_\Lambda=1-\Omega_0$. According to the semi-analytic treatment of the self-similar solution for the Einstein–de Sitter universe by Bertschinger (1985), the accretion shock of BM with $\gamma=5/3$ forms very close to the first caustic of dM, and the flow upstream to the accretion shock and the first caustic is identical regardless of whether it is collisional or collisionless. Thus, we have assumed that the position of the accretion shock can be approximated by that of the first caustic and the accretion velocity of BM outside the accretion shock by that of DM outside the first caustic. Since self-
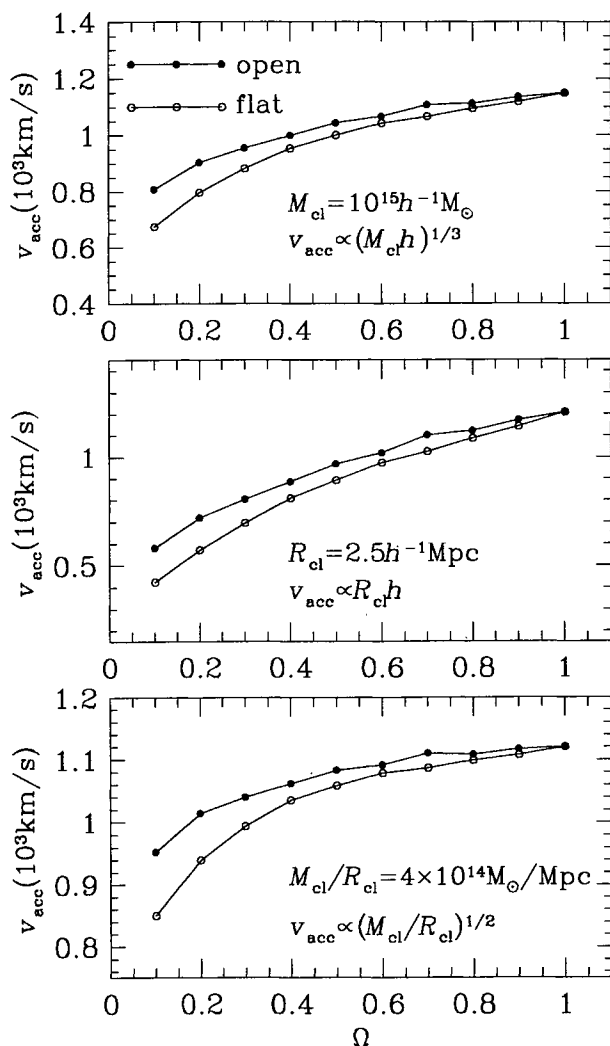

Figure 5. Present accretion velocity, v_{acc}, for clusters with the present mass $M_{cl}(z=0)=10^{15}\,h^{-1}\,M_\odot$ (the first panel), for clusters with the present radius $R_{cl}(z=0)=2.5\,h^{-1}$ Mpc (the second panel), and for clusters with the present $M_{cl}/R_{cl}=4\times10^{14}\,M_\odot$ Mpc^{-1} (third panel) in the open universes (filled circles) and the flat universes (open circles) with different Ω_0. That with $\Omega_0=1$ represents the values in the Einstein–de Sitter universe.
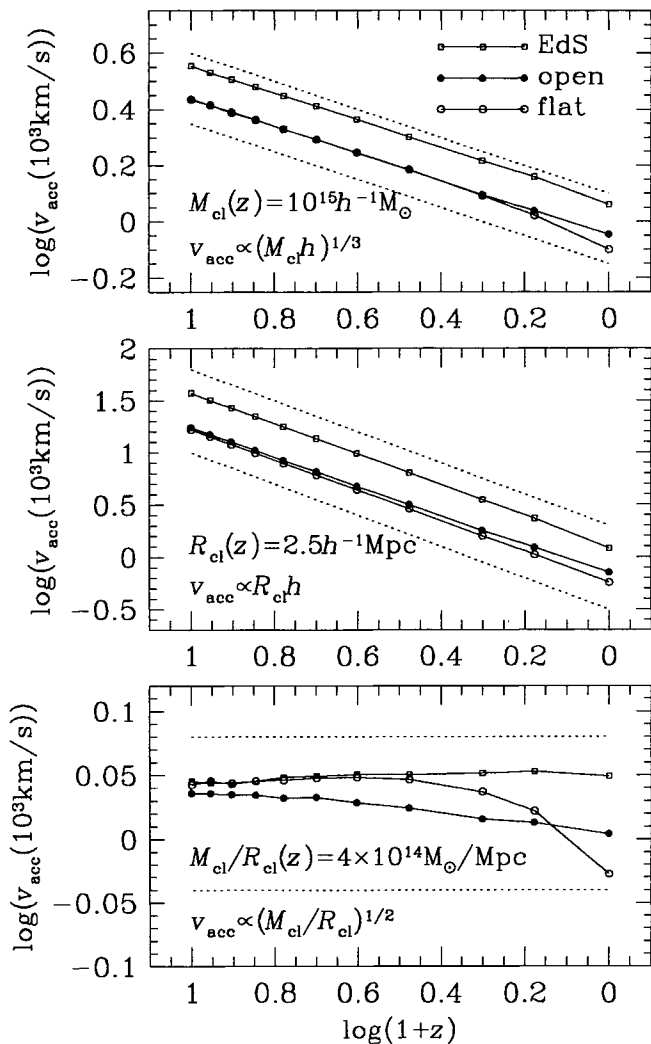
Figure 6. Accretion velocity, v_{acc}, as a function of redshift in the Einstein–de Sitter universe (open squares), in the open universe with $\Omega_0 = 0.2$ (filled circles), and in the flat universe with $\Omega_0 = 0.2$ (open circles). The first panel is for clusters with a mass at given z, $M_{cl}(z) = 10^{15} h^{-1}$ M$_\odot$. The second panel is for clusters with a radius at given z, $R_{cl}(z) = 2.5 h^{-1}$ Mpc. The third panel is for clusters with M_{cl}/R_{cl} at given z, $M_{cl}/R_{cl}(z) = 4 \times 10^{14}$ M$_\odot$ Mpc^{-1}. The dotted lines represent the power-law evolution in the exact self-similar solution in the Einstein–de Sitter universe (Bertschinger 1985).

similar solutions do not exist for $\Omega_0 \neq 1$ universes, we have used a one-dimensional, spherical, N-body code to study the properties of accreting matter.

The accretion velocity on to a cluster with a given initial perturbation has decreased as the universe expands in all cosmological models. In the Einstein–de Sitter universe it has followed $v_{acc} \propto (1 + z)^{1/6}$ (Bertschinger 1985), while in low density universes it decreases faster with time, especially at low redshifts (see Fig. 2). This is related to the smaller deceleration of the expanding background.

The properties of accretion flows around the clusters of the same characteristic (mass, radius or temperature) will depend on the cosmological parameters, Ω_0 and Λ, since the accretion rate is affected by the expansion rate of the back-

ground universe. The accretion velocity is smaller in a lower density universe and even smaller in a non-zero Λ universe. For clusters of a given mass at given redshift, the present accretion velocity in the low-density universe with $\Omega_0 \geq 0.1$ is smaller by up to ~ 41 per cent than that in the Einstein–de Sitter universe. For clusters of a given radius at given redshift, the present accretion velocity in the low-density universe with $\Omega_0 \geq 0.1$ is smaller by up to ~ 65 per cent than that in the Einstein–de Sitter universe. Hence, if the accretion velocity of infalling matter around clusters can be measured along with their mass and radius, then it could be used to discriminate the different cosmological models.

However, for clusters of a given temperature or given M_{cl}/R_{cl}, the present value of the accretion velocity as well as its evolution depend on the cosmological model rather weakly. According to the self-similar solution of Bertschinger (1985), in the Einstein–de Sitter universe, for clusters of a given temperature, the accretion velocity at present is given as $v_{acc} = 1.31 \times 10^3$ km s^{-1} $(T_{cl}/6.06 \text{ keV})^{1/2}$, and it has been constant through the evolution of the universe. In the universes with smaller Ω_0, the present accretion velocity is smaller by up to ~ 24 per cent in the models considered here with $0.1 \leq \Omega_0 \leq 1$. However, this difference decreases to a few per cent at high redshifts (see Figs 5 and 6). Thus, it would be difficult to use the accretion velocity of clusters with a given temperature to discriminate among the cosmological models.

However, this has an important implication for the model of the origin of ultrahigh-energy cosmic rays that the acceleration of protons in accretion shock around clusters can contribute significantly to the observed particle flux above 3×10^{18} eV (Kang, Ryu & Jones 1996; Kang, Rachen & Biermann 1996). We have shown in this paper that the matter accretion and the accretion shock around clusters are universal for all cosmological models, although the accretion regime is less strong in lower density universes. The shock velocity $v_s = (4/3)v_{acc}$ for the rich clusters of $T_{cl} = 10$ keV, for example, is estimated to be 2200 km s^{-1} in the Einstein–de Sitter universe, which is enough for the model to work. The results in this paper imply that the model might be extended to all cosmologically viable universes of low density, since the reduction in the shock velocity is no more than ~ 24 per cent.

The region of clusters observed by either optical or X-ray observations ($r \lesssim 1$–$1.5 h^{-1}$ Mpc) is inside the first caustic or the accretion shock ($R_{cl} \sim 1$–$3 h^{-1}$ Mpc for $T_{cl} \sim 1$–10 keV). Although the existence of hot gas heated by the accretion shocks has been shown clearly in most cosmological simulations including hydrodynamics for any variants of cosmological models (Kang et al. 1994; Cen & Ostriker 1994; Navarro, Frenk & White 1995), any direct observations of gas near the shock would not be possible at present because of low surface brightness. However, it has been suggested that the unbound hot gas of 10^5–10^6 K around clusters and groups heated by the large-scale accretion shocks is a major component of the IGM which emits mostly at the soft X-ray region below 1 keV (Ostriker & Cen 1996). This prediction might be tested by looking for the spatial correlation between the soft X-ray cosmic background radiation and the observed large-scale structure.

On the other hand, the infalling clouds of unshocked, warm gas may be identified through the absorption lines of

quasars which are located inside clusters of galaxies. This warm low density gas of 10^4–10^5 K is photoionized by the diffuse radiation from the hot post-shock gas and the diffuse cosmic background radiation. In some studies (for example, Weymann et al. 1979; Foltz et al. 1986), the C IV absorption systems of quasar emission lines with $|z_{abs} - z_{QSO}| < 3000$ km s^{-1} are interpreted as clouds associated with rich clusters where the quasars reside. The characteristics of these systems of C IV absorbers are different from those of the typical intervening C IV absorbers. It was noted that the velocity difference is somewhat too large compared with the typical velocity dispersion of galaxies (400–1200 km s^{-1}) in rich clusters (Foltz et al. 1986). The accretion velocity, however, is a bit larger than the galaxy velocity dispersions, since it is given by $v_{acc} = 1.31 \times 10^3$ km s^{-1} $(T_{cl}/6.06 \text{ keV})^{1/2}$ in the Einstein–de Sitter universe. Thus it is possible that these absorption systems are in fact the infalling clumps of gas upstream of the accretion shock.

In follow-up papers we will study the properties and statistics of three-dimensional accretion flows in simulated universes by analysing the data from three-dimensional hydrodynamic simulations of various cosmological models (for example, Kang et al. 1994; Cen & Ostriker 1994). These simulations have been performed by a high-resolution, grid-based, Eulerian code (Ryu et al. 1993) which resolves the shock discontinuity in 2–3 cells and is designed specifically to handle the flows with supersonic bulk motions. Thus, the low-density regions around caustics and shocks are well represented in these simulations, even though the high-density core region of clusters might be under-resolved (Kang et al. 1994). The present one-dimensional study will provide some useful guidance for such studies.

ACKNOWLEDGMENTS

REFERENCES

Bahcall N. A., Cen R., 1992, ApJ, 398, L81
Bardeen J. M., Bond J. R., Kaiser M., Szalay A. S., 1986, ApJ, 304, 15
Bertschinger E., 1985, ApJS, 58, 39
Castander F. J. et al., 1995, Nat, 377, 39
Cen R., Ostriker J. P., 1994, ApJ, 429, 4
Crone M., Evrard A. E., Richstone D. O., 1994, ApJ, 434, 402
Eke B. R., Cole S., Frenk C. S., 1996, MNRAS, in press
Evrard A. E., Metzler C. A., Navarro J. F., 1996, ApJ, 469, 494
Fillmore J. A., Goldreich P., 1984, ApJ, 281, 1
Foltz C. B., Weymann R. J., Peterson B. M., Sun L., Malkan M. A., Chaffee F. H., Jr, 1986, ApJ, 307, 504
Forman W., Jones C., 1982, ARA&A, 20, 547
Hoffman Y., Shaham J., 1985, ApJ, 297, 16
Kang H., Cen R., Ostriker J. P., Ryu D., 1994, ApJ, 428, 1
Kang H., Rachen J., Biermann P., 1996, MNRAS, in press
Kang H., Ryu D., Jones T. W., 1996, ApJ, 456, 422

Kitayama T., Suto Y., 1996, MNRAS, in press (astro-ph/9602076)
Lacey C., Cole S., 1994, MNRAS, 271, 676
Lubin L. M., Cen R., Bahcall N. A., Ostriker J. P., 1996, ApJ, 460, L10
Luppino G. A., Gioia I. M., 1995, ApJ, 445, L77
Navarro J., Frenk C. S., White D. M., 1995, MNRAS, 275, 720
Ostriker J. P., Cen R., 1996, ApJ, 464, 270
Ostriker J. P., Steinhardt P. J., 1995, Nat, 377, 600
Peebles P. J. E., 1993, Principles of Physical Cosmology. Princeton Univ. Press, Princeton
Press W. H., Schechter P., 1974, ApJ, 187, 425
Ryu D., Ostriker J. P., Kang H., Cen R., 1993, ApJ, 414, 1
Tsai J. C., Buote D. A., 1996, MNRAS, 282, 77
Viana P. T. P., Liddle A. R., 1996, MNRAS, 281, 323
Weymann R. J., Williams R. E., Peterson B. M., Turnshek D. A., 1979, ApJ, 234, 33
White S. D. M., Efstathiou G., Frenk C. S., 1993, MNRAS, 262, 1023

APPENDIX A: BASIC EQUATIONS

In comoving coordinates, the equations to describe the evolution of the collisionless DM particles are written as

$$\frac{d\mathbf{r}}{dt} = \frac{1}{a}\mathbf{u}, \tag{A1}$$

and

$$\frac{d\mathbf{u}}{dt} = -\frac{\dot{a}}{a}\mathbf{u} - \frac{1}{a}\nabla\phi, \tag{A2}$$

where $\mathbf{r}$ is the comoving position, $\mathbf{u}$ is the proper peculiar velocity, ϕ is the proper peculiar gravitational potential, and a is the cosmic expansion parameter. The potential is given by the Poisson equation

$$\nabla^2\phi = \frac{a_0^3}{a}4\pi G[\rho(\mathbf{r}) - \bar{\rho}], \tag{A3}$$

where $\rho(\mathbf{r})$ is the comoving matter density, $\bar{\rho}$ is the average comoving matter density, and a_0 is the present value of the expansion parameter.

The expansion parameter and its time derivative (or the expansion rate) are calculated as a function of time by the following equations (see Peebles 1993).

$$\frac{a}{a_0} = \left(\frac{3}{2}H_0 t\right)^{2/3}, \qquad \text{for Einstein–de Sitter} \tag{A4}$$

$$\frac{a}{a_0} = \frac{\Omega_0}{2(1-\Omega_0)}(\cosh\eta - 1)$$

and

$$H_0 t = \frac{\Omega_0}{2(1-\Omega_0)^{3/2}}(\sinh\eta - \eta), \qquad \text{for open} \tag{A5}$$

$$\frac{a}{a_0} = \left(\frac{\Omega_0}{1-\Omega_0}\right)^{1/3}\sinh^{2/3}\left(\frac{3}{2}\sqrt{1-\Omega_0}H_0 t\right), \qquad \text{for flat} \tag{A6}$$

and

$$\left(\frac{\dot{a}}{a}\right)^2 = H_0^2 \left[\Omega_0 \left(\frac{a_0}{a}\right)^3 + \Omega_R \left(\frac{a_0}{a}\right)^2 + \Omega_\Lambda\right]. \tag{A7}$$

Here, H_0 is the present value of the Hubble parameter and Ω_0, Ω_R, and Ω_Λ are constants. The density parameter is given as

$$\Omega_0 = \frac{8\pi G\bar{\rho}}{3H_0^2}, \tag{A8}$$

which is the present average mass density in terms of the critical density. The parameter associated with the radius of curvature R is given as

$$\Omega_R = \frac{1}{(a_0 H_0 R)^2}, \tag{A9}$$

which is positive for an open universe and zero for others. The parameter associated with the cosmological parameter Λ is given as

$$\Omega_\Lambda = \frac{\Lambda}{3H_0^2}, \tag{A10}$$

which is positive for a flat universe and zero for others. The three parameters give the relative contributions to the present expansion rate by satisfying

$$\Omega_0 + \Omega_R + \Omega_\Lambda = 1. \tag{A11}$$

We have solved numerically the equations governing the evolution for the DM particles [equations (A1)–(A3)], simultaneously with the equations describing the background universe [equations (A4)–(A7)]. In the next appendix, we describe the scheme used.

APPENDIX B: NUMERICAL SCHEME

In the one-dimensional spherical code to calculate the time integration of the equations of motion [equations (A1)–(A2)], we have adopted the second-order accurate Lax–Wendroff scheme instead of the more popular leapfrog scheme, since the code was originally designed to be a part of a one-dimensional code which follows the evolution of the baryonic matter as well as that of the DM in a way

parallel to the three-dimensional cosmological hydro-dynamic code (Ryu et al. 1993). So the update of the position and velocity of the particle i from n time step to $n + 1$ is carried out by the following two steps:

$$r_i^{n+1/2} = r_i^n + \frac{\Delta t^n}{2} \frac{u_i^n}{a^n}, \tag{B1}$$

$$u_i^{n+1/2} = u_i^n - \frac{\Delta t^n}{2} \frac{\dot{a}^n}{a^n} u_i^n + \frac{\Delta t^n}{2} g_i^n, \tag{B2}$$

and

$$r_i^{n+1} = r_i^n + \Delta t^n \frac{u_i^{n+1/2}}{a^{n+1/2}}, \tag{B3}$$

$$u_i^{n+1} = u_i^n - \Delta t^n \frac{\dot{a}^{n+1/2}}{a^{n+1/2}} u_i^{n+1/2} + \Delta t^n g_i^{n+1/2}, \tag{B4}$$

where g denotes the gravitational force. With the variables normalized with the present age of the universe, t_0, the comoving size of the box, L_0, and $\bar{\rho}$, g_i^n is calculated with

$$g_i^n = -\frac{3}{8\pi} (H_0 t_0)^2 \Omega_0 \frac{a_0^3}{(a^n)^2} \frac{\delta M(r_i^n)}{[\max(r_i^n, \varepsilon)]^2}, \tag{B5}$$

where $\delta M(r_i^n)$ is the mass excess inside r_i^n. Similarly, $g_i^{n+1/2}$ is calculated with the quantities at $n + 1/2$. Here ε is the smoothing parameter which prevents the time-step becoming too short, or prevents the particles being accelerated anomalously for a given time-step around the origin.

A particle, which is placed close to and approaches the origin, can pass the origin in the half time-step $(n + 1/2)$. Then, the absolute value of its position is used to calculate the gravitational force at the half time-step. If a particle passes the origin after the full time-step $(n + 1)$, its position and velocity are reset to their negative values.

The time-step, Δt, is determined so that $\Delta a/a$ is constant in each time-step. In all the calculations discussed in this paper, we have used 10^4 particles and $\Delta a/a = 10^{-3}$. With these, $\varepsilon = 5 \times 10^{-2}$ in unit of L_0 assures that the gravitational time-scale in the core region with $r < \varepsilon$ is comfortably small compared to the time-step along the whole calculation. However, the force smoothing makes the density smoothed in the core region with $r \lesssim \varepsilon$ (see Section 2).